Observer-Based Ripple Force Compensation for Linear Hybrid Stepping Motor Drives

Tai-Sik Hwang, *Student Member, IEEE*, and Jul-Ki Seok, *Member, IEEE*

***Abstract*—This paper describes our research on a force ripple compensation and closed-loop position control scheme using linear hybrid stepping motors (LHSMs) with significant thrust vibrations. In order to estimate unobservable force ripple components, we propose the Jacobian linearization observer that guarantees the convergence of state estimates into true states. For the precise control of velocity and position, an input–output feedback linearization controller is derived from a nonlinear position-dependent model of the LHSM based on elaborate reluctance network analysis. In addition, we discuss the separation principle used to separate the observer design from the controller design. Common problems associated with the force ripple, such as the positioning error, mechanical stress, and acoustic noise, are efficiently handled using the proposed active damping control scheme. Experimental results show that the positioning accuracy is significantly improved through a closed-loop control while restraining the thrust ripple.**

***Index Terms*—Feedback linearization controller, Jacobian linearization observer, linear hybrid stepping motors (LHSMs), separation principle, thrust vibrations.**

I. Introduction

THERE HAS been considerable interest over the years in the development of high-speed/high-precision linear motion control systems, and this is because of the increasing demand for higher productivity and better product quality in advanced manufacturing industries such as industrial process machinery, computer peripherals, and robotic systems. Among various electric motor drives, linear hybrid stepping motors (LHSMs) are naturally thought to be most applicable to applications requiring high speed, low cost, and simple control [1]–[3]. Most LHSMs have a compact structure consisting of a permanent magnet (PM) mover with armature coils and a thin steel platen with many teeth. These motors are very strong competitors for use in long track applications. In these applications, the simple and inexpensive platen structure results in a great reduction of initial production costs. They also have other distinctive features such as ruggedness, high reliability, and ripple-free holding force at an aligned position [1]. The advantages of the LHSMs, aforementioned, are considered to be indispensable conditions for control systems requiring multiaxis movements.

However, despite their attractive features, the LHSM has significant thrust vibrations during position-to-position movement due to the space harmonics of the permeance distribution [2]. In the case of the smooth control required at low speeds, such as the image observation system using a camera mounted directly on the LHSMs or servo applications, the force ripple reduction becomes the main issue. The periodic thrust ripple causes position error of more than ± 20 μm, mechanical vibration, and acoustic noise, which makes the control performance worse and sometimes leads to destruction of mechanical systems. Consequently, their use in servosystems, which requires smooth/quiet operation and accurate position control of less than ± 2.5 μm at low speeds, has been limited.

Recently, some attempts have been made to achieve high-precision performances with LHSMs using a closed-loop current control [2]. Further improvements can be achieved by means of motor position/velocity feedback, as for example, converting the LHSM drive into a true closed-loop servo system [4]–[7]. Unfortunately, these methods are not based on the actual motor modeling with periodic force oscillations. As a consequence, the compensation results may not be promising. Thus, for the high-precision control performance in all operating regions, the force ripple should be suppressed using an online compensation scheme based on an accurate motor modeling.

We explored an alternative approach to eliminate the force ripple through an interesting design structure employing a dual PM topology [3]. In this approach, all the magnetic poles of the motor have permeances with a $\pi/4$-multiple pitch difference. This motor is called a $\pi/4$-multiple-pitched LHSM. Cogging forces in opposite directions, because of the tendency of two PMs to align themselves along the direction of minimum reluctance, cancel each other so that the total pulsation is weakened. A limitation of this type of design approach is that real motors are known to contain design imperfections and nonlinear magnetics. They, in turn, give rise to the cogging force in the motor. Nevertheless, the $\pi/4$-multiple-pitched LHSM, with the inherent low detent force, is a strong candidate to use in high-performance motion control applications.

This paper describes our proposal for an active ripple-reduction scheme for an LHSM. Our proposal is based on a position-dependent nonlinear model developed through an elaborate reluctance network analysis. To reduce the vibration from the ripple force, the unobservable ripple components, at an arbitrary mover position, are dynamically estimated from

Manuscript received February 11, 2006; revised October 22, 2006. This work was supported by KESRI (R-2005-B-143), which is funded by MOCIE (Ministry of Commerce, Industry, and Energy).

T.-S. Hwang is with Robostar Company Ltd., Anyang 431-836, Korea (e-mail: hwangts@robostar.co.kr).

J.-K. Seok is with the School of Electrical Engineering, Yeungnam University, Gyeongsan 712-749, Korea (e-mail: doljk@ynu.ac.kr).

Color versions of one or more of the figures in this paper are available online at http://ieeexplore.ieee.org.

Digital Object Identifier 10.1109/TIE.2007.900344

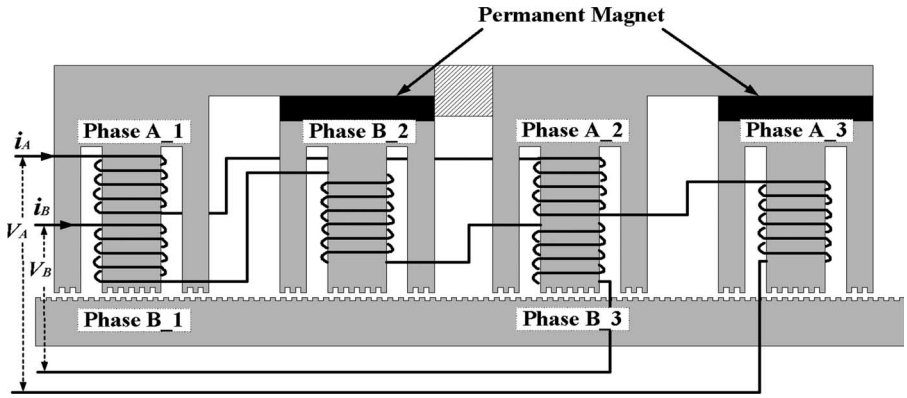

Fig. 1. Structure of $\pi/4$-multiple-pitched LHSM.

a Jacobian linearization observer. They are then injected so as to cancel the ripple force in a feedforward manner. A nonlinear state feedback linearization controller is applied, and the stability of this closed-loop system, including the observer, is demonstrated by using Lyapunov stability theory. In combination with the observer, this approach can effectively deal with the precise closed-loop position control of an LHSM with significant thrust vibrations. Experimental results are presented to prove the effectiveness of the proposed vibration-rejecting scheme.

II. LHSM Modeling With Magnetic Imbalances

The schematic of a $\pi/4$-multiple-pitched LHSM is shown in Fig. 1, where the residual flux density of the PM with its magnetization upward is 1.145 T. The first and third magnetic poles have a two-phase coil winding structure, respectively. Each phase coil turn is $1/\sqrt{2}$ times those of main windings wound at the second and fourth poles. Such compound windings are revealed in order to make enhancements in the force-producing characteristics of the LHSM [3].

A. Magnetic Imbalance

Fig. 2 shows the measured back-EMF voltage at the motor terminal when the mover is moved manually. The difference in the back-EMF voltage is thought to result from the undesirable magnetic coupling between phase B_2 and phase A_3 in Fig. 2, which is often assumed to be separated to each other. In addition, the PM flux density is not uniform in each nonideal iron core with a finite relative permeability because PMs are not located at the center position of each core in this structure. This will lead us to a better understanding of the force ripple phenomenon mainly generated by the inherently unbalanced magnetic structure of the LHSM [6]. The distortion of the flux distribution may have a detrimental influence on the actual motor back-EMF, as shown in Fig. 2. Since the back-EMF is asymmetrical, the motor force has a second-order harmonic oscillation if the A- and B-phase currents are balanced. Therefore, for a more accurate prediction of the thrust ripple, the magnetic imbalance of the LHSM has to be properly reflected in the reluctance network method.

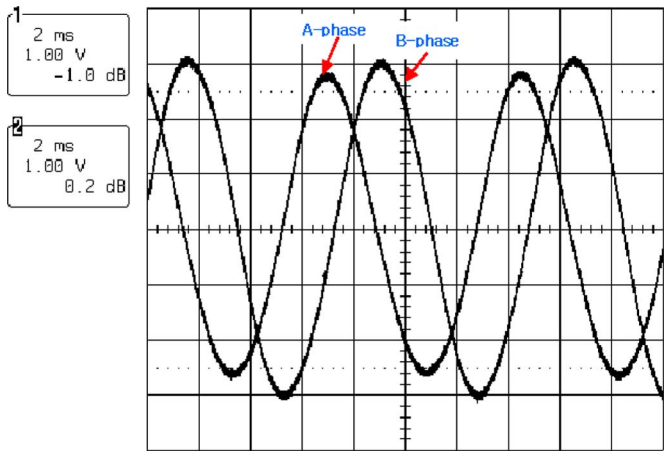

Fig. 2. Measured back-EMF waveforms while controllers are disabled.

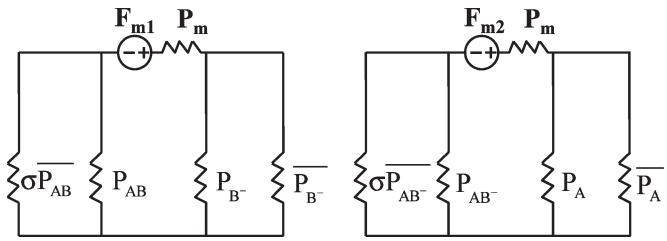

Fig. 3. Modified magnetic circuit with magnetic asymmetry.

B. LHSM Modeling With Magnetic Asymmetry

To consider the asymmetry of flux distribution properly, it is desirable to assign two different magnetic motive forces (F_{m1} and F_{m2}) and insert a branch with an asymmetric factor σ in the original magnetic circuit [3], as shown in Fig. 3, where P_m represents the permeance of the PM.

Neglecting high-order harmonic components [3], the permeance in each branch is given by

$$P_{AB} = P_o + \sum_{n=1}^{5} P_n \cos n\left(\theta - \frac{\pi}{4}\right) \tag{1}$$

$$\overline{P_{AB}} = P_o + \sum_{n=1}^{5} P_n \cos n\left(\theta - \frac{\pi}{4} - \pi\right) \tag{2}$$

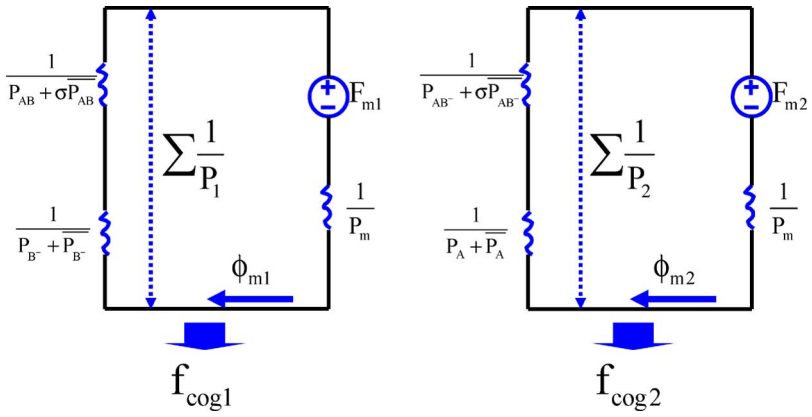

Fig. 4. Simplified magnetic equivalent circuit.

$$P_{B^-} = P_o + \sum_{n=1}^{5} P_n \cos n\left(\theta - \frac{\pi}{2}\right) \tag{3}$$

$$\overline{P_{B^-}} = P_o + \sum_{n=1}^{5} P_n \cos n\left(\theta - \frac{\pi}{2} - \pi\right) \tag{4}$$

$$P_{AB^-} = P_o + \sum_{n=1}^{5} P_n \cos n\left(\theta - \frac{3\pi}{4}\right) \tag{5}$$

$$\overline{P_{AB^-}} = P_o + \sum_{n=1}^{5} P_n \cos n\left(\theta - \frac{3\pi}{4} - \pi\right) \tag{6}$$

$$P_A = P_o + \sum_{n=1}^{5} P_n \cos n(\theta - \pi) \tag{7}$$

$$\overline{P_A} = P_o + \sum_{n=1}^{5} P_n \cos n(\theta) \tag{8}$$

$$\theta = \gamma x = \frac{2\pi}{p_t} x \tag{9}$$

where p_t is the pole pitch, and x indicates the mover position.

A simplified magnetic circuit is redrawn and shown in Fig. 4 under the conditions of $P_o \gg (\sigma - 1/\sigma + 1)P_1$ and $P_o \gg P_2, P_3, P_4, P_5$ [4]. Then, the total permeance can be calculated as in (10) and (11) shown at the bottom of the page.

By utilizing the permeance expressions in (10) and (11), the stored magnetic coenergy, W'_{m1} and W'_{m2}, in the two circuits in Fig. 4 can be easily obtained as $(1/2)(F_{m1}/P_m)^2(1/\sum P_1)$ and $(1/2)(F_{m2}/P_m)^2(1/\sum P_2)$, respectively.

After taking the partial derivative of the stored coenergy, the cogging force generated by each part of the LHSM under consideration is given by

$$f_{\text{cog1}} = \frac{\partial W'_{m1}}{\partial x} = \left(\frac{2\pi}{p_t}\right)\frac{\phi_{m1}^2}{2P_o^2} \times \begin{pmatrix} \frac{\sigma-1}{(\sigma+1)^2}P_1 \sin\left(\theta - \frac{\pi}{4}\right) - P_2 \sin 2\theta - \frac{2P_2}{\sigma+1}\cos 2\theta \\ + \frac{3(\sigma-1)}{(\sigma+1)^2}P_3 \sin\left(3\theta - \frac{\pi}{4}\right) + \frac{2(\sigma-1)}{\sigma+1}P_4 \sin 4\theta \end{pmatrix} \tag{12}$$

$$f_{\text{cog2}} = \frac{\partial W'_{m2}}{\partial x} = \left(\frac{2\pi}{p_t}\right)\frac{\phi_{m2}^2}{2P_o^2} \times \begin{pmatrix} \frac{\sigma-1}{(\sigma+1)^2}P_1 \sin\left(\theta + \frac{\pi}{4}\right) + P_2 \sin 2\theta + \frac{2P_2}{\sigma+1}\cos 2\theta \\ + \frac{3(\sigma-1)}{(\sigma+1)^2}P_3 \sin\left(3\theta + \frac{\pi}{4}\right) + \frac{2(\sigma-1)}{\sigma+1}P_4 \sin 4\theta \end{pmatrix}. \tag{13}$$

The resultant force of the LHSM with the magnetic asymmetry has the form of

$$F_{\text{ripple}} = f_{\text{cog1}} + f_{\text{cog2}} = \sum_{n=1}^{4} f_n \cos(n\gamma x + \delta_n). \tag{14}$$

The first-, second-, third-, and fourth-order harmonic components of the permeance generate the same order ripple force.

$$\frac{1}{\sum P_1} \cong \frac{1}{P_o^2}\begin{pmatrix} \frac{\sigma+3}{2(\sigma+1)}P_o - \frac{\sigma-1}{(\sigma+1)^2}P_1 \cos\left(\theta - \frac{\pi}{4}\right) + \frac{P_2}{2}\cos 2\theta - \frac{P_2}{\sigma+1}\sin 2\theta \\ - \frac{\sigma-1}{(\sigma+1)^2}P_3 \cos\left(3\theta - \frac{\pi}{4}\right) - \frac{\sigma-1}{2(\sigma+1)}P_4 \cos 4\theta \end{pmatrix} \tag{10}$$

$$\frac{1}{\sum P_2} \cong \frac{1}{P_o^2}\begin{pmatrix} \frac{\sigma+3}{2(\sigma+1)}P_o - \frac{\sigma-1}{(\sigma+1)^2}P_1 \cos\left(\theta + \frac{\pi}{4}\right) - \frac{P_2}{2}\cos 2\theta + \frac{P_2}{\sigma+1}\sin 2\theta \\ - \frac{\sigma-1}{(\sigma+1)^2}P_3 \cos\left(3\theta + \frac{\pi}{4}\right) - \frac{\sigma-1}{2(\sigma+1)}P_4 \cos 4\theta \end{pmatrix} \tag{11}$$

This force's corresponding amplitude is proportional to the magnetic imbalance.

By using the position-dependent ripple force model, the mechanical equation of the motor is as follows:

$$\frac{d\nu}{dt} = \frac{1}{m}(F_e + F_{\text{ripple}}) \tag{15}$$

where ν is the motor velocity, m indicates the system mass, and F_e represents the instantaneously generated force.

To suppress the force disturbance, ripple components need to be observed from currents, velocity feedback, and system mass. For the purpose of designing an observer, a state-space representation is first required. From (15), the first-order component is described as

$$\begin{aligned} x_1 &= x \\ \dot{x}_1 &= x_2 \\ &= \nu \\ x_3 &= f_1 \cos(\gamma x + \delta_1) \\ x_4 &= -\frac{f_1}{\gamma}\sin(\gamma x + \delta_1). \end{aligned} \tag{16}$$

The next nonlinear state-space form can be derived from (16) as follows:

$$\begin{aligned} \dot{x}_3 &= -\gamma\nu f_1 \sin(\gamma x + \delta_1) = \gamma^2 x_2 x_4 \\ \dot{x}_4 &= -\nu f_1 \cos(\gamma x + \delta_1) = -x_2 x_3. \end{aligned} \tag{17}$$

Then, the overall state equation can be obtained with a straightforward extension

$$\begin{aligned} \dot{\mathbf{x}} &= f(\mathbf{x}) + g(\mathbf{x})u \\ y &= h(\mathbf{x}) \end{aligned}$$

$$f(\mathbf{x}) = \begin{bmatrix} x_2 \\ \frac{1}{m}(x_3 + x_5 + x_7 + x_9) \\ \gamma^2 x_2 x_4 \\ -x_2 x_3 \\ 4\gamma^2 x_2 x_6 \\ -x_2 x_5 \\ 9\gamma^2 x_2 x_8 \\ -x_2 x_7 \\ 16\gamma^2 x_2 x_{10} \\ -x_2 x_{10} \end{bmatrix}$$

$$g(\mathbf{x}) = \begin{bmatrix} 0 \\ \frac{1}{m} \\ 0 \\ 0 \\ 0 \\ 0 \\ 0 \\ 0 \\ 0 \\ 0 \end{bmatrix}$$

$$\begin{aligned} h(\mathbf{x}) &= x_1 \\ F_{\text{ripple}} &= x_3 + x_5 + x_7 + x_9. \end{aligned} \tag{18}$$

A block diagram of the LHSM model, taking into account the ripple force effect, is illustrated in Fig. 5. In this diagram, F_{L} denotes the external load force, and F_{fric} is the friction disturbance of the system.

III. Observer-Based Ripple Force Reduction Scheme

A. Estimation of Ripple Force Component

Contrary to linear systems, the nonlinear observer problem of (18) has not yet been wholly solved in the general sense. There are several particular classes of nonlinear estimation solutions [8]. Here, we choose the Jacobian linearization observer that is designed as (19) by using the first-order linear approximation of the system at the origin

$$\begin{aligned} \dot{\hat{x}}_2 &= \frac{1}{m}(\hat{x}_3 + \hat{x}_5 + \hat{x}_7 + \hat{x}_9) + \frac{1}{m}F_e + l_1(\nu - \hat{x}_2) \\ \dot{\hat{x}}_3 &= \gamma^2\nu\hat{x}_4 + l_2(\nu - \hat{x}_2) - (\dot{x}^* - \nu) \\ \dot{\hat{x}}_4 &= -\nu\hat{x}_3 \\ \dot{\hat{x}}_5 &= 4\gamma^2\nu\hat{x}_6 + l_3(\nu - \hat{x}_2) - (\dot{x}^* - \nu) \\ \dot{\hat{x}}_6 &= -\nu\hat{x}_5 \\ \dot{\hat{x}}_7 &= 9\gamma^2\nu\hat{x}_8 + l_4(\nu - \hat{x}_2) - (\dot{x}^* - \nu) \\ \dot{\hat{x}}_8 &= -\nu\hat{x}_7 \\ \dot{\hat{x}}_9 &= 16\gamma^2\nu\hat{x}_{10} + l_5(\nu - \hat{x}_2) - (\dot{x}^* - \nu) \\ \dot{\hat{x}}_{10} &= -\nu\hat{x}_9 \\ \hat{F}_{\text{ripple}} &= \hat{x}_3 + \hat{x}_5 + \hat{x}_7 + \hat{x}_9 \end{aligned} \tag{19}$$

where $L = [l_1\ l_2\ l_3\ l_4\ l_5]^{\text{T}}$ is chosen such that $(\partial f/\partial \mathbf{x})(0) + K(\partial h/\partial \mathbf{x})(0)$ is a Hurwitz matrix [9]. This observer design method requires neither an integration of partial differential equations nor a knowledge of the input derivatives. That leads to an advantage of easy implementation of our proposed method.

B. Feedback Linearization for Position and Velocity Control

Feedback linearization has been recognized as a powerful method for nonlinear system; hence, it is natural to apply feedback linearization to systems with the expectation that the feedback linearization will cancel out nonlinear terms. From (15) and (18)

$$\ddot{y} = \dot{x}_2 = \frac{1}{m}(x_3 + x_5 + x_7 + x_9) + \frac{1}{m}F_e^* \tag{20}$$

and choosing the new input z as

$$z = \ddot{x}^* + k_1(\dot{x}^* - \nu) + k_2(x^* - x) = \ddot{x}^* + k_1\dot{e} + k_2 e \tag{21}$$

where x^* represents the position command. With k_1 and k_2 being positive constants, the tracking error of the closed-loop system is given by

$$\ddot{e} + k_1\dot{e} + k_2 e = 0 \tag{22}$$

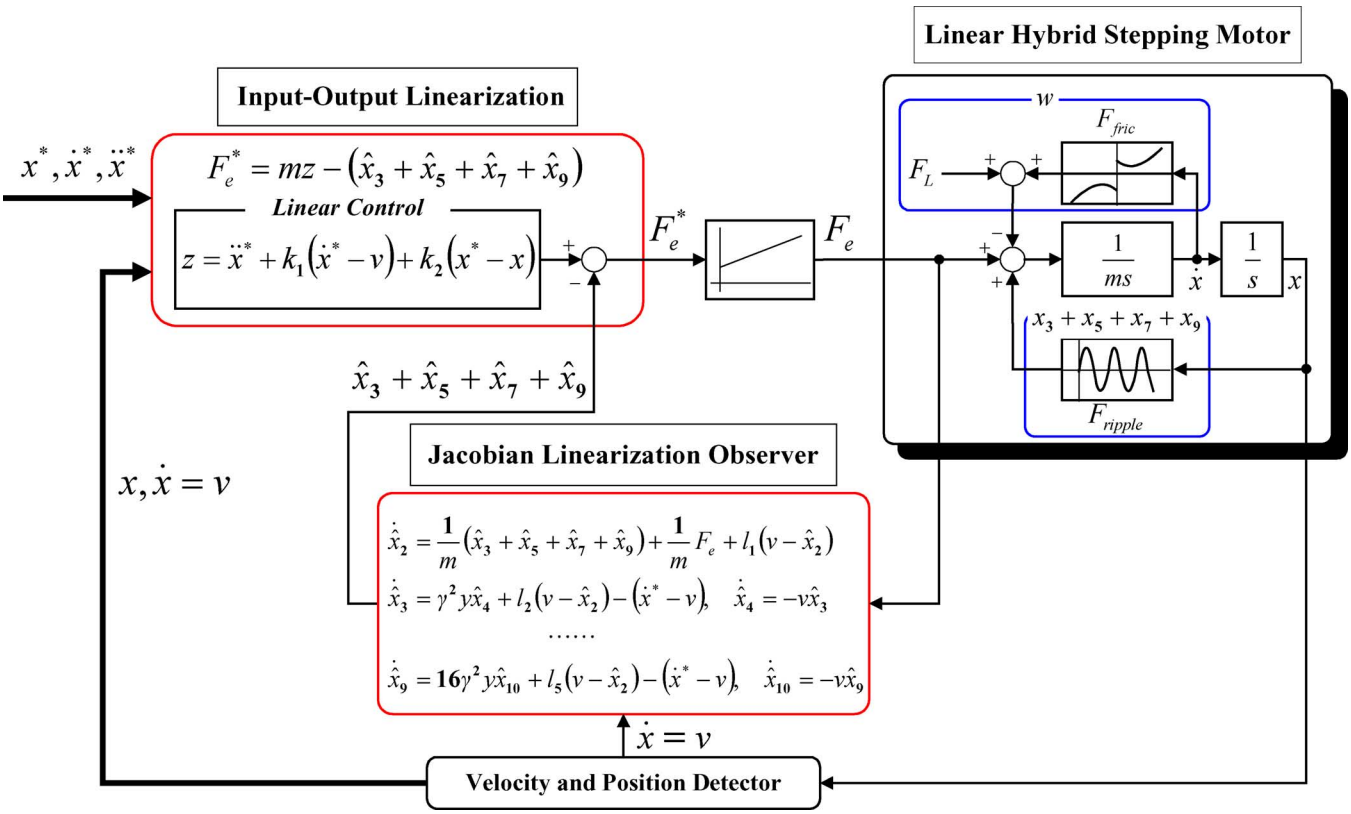

Fig. 5. Overall control block diagram for ripple force compensation.

where k_1 and k_2 are chosen such that $s^2 + k_1 s + k_2 = 0$ is a Hurwitz polynomial.

From (16) and (17), notice that the internal dynamics is bounded as

$$\left.\begin{array}{l} |x_{2n-1}| \le f_n \\ |x_{2n+2}| \le \frac{f_n}{n\gamma} \end{array}\right\}, \qquad n = 1, 2, 3, 4. \tag{23}$$

Fig. 5 shows the overall control block diagram of the proposed scheme to mitigate the ripple force. In the proposed method, the compensating signal is added to the output of the input–output linearization controller that automatically adjusts the motor force in order to reduce the force pulsation.

A friction or load disturbance in Fig. 5 is separately identified. It could be possible to design a control scheme that would cancel the disturbance [10], [11]. Although this problem is beyond the scope of this paper, the robustness of the proposed scheme was tested in the presence of an unknown friction disturbance.

C. Estimated State Feedback and Closed-Loop Stability

Unfortunately, unlike the case of linear systems, it is not straightforward to combine the observer with the predesigned state feedback law for the stability of nonlinear systems [12]. In other words, the separation design of the controller and observer cannot guarantee the closed-loop stability for nonlinear systems. In this case, the ripple force components are not measured. The error dynamics becomes

$$\begin{aligned}
\dot{e}_1 &= e_2 \\
\dot{e}_2 &= -k_1 e_2 - k_2 e_1 + \frac{1}{m}(\tilde{x}_3 + \tilde{x}_5 + \tilde{x}_7 + \tilde{x}_9) \\
\dot{\tilde{x}}_2 &= -l_1 \tilde{x}_2 + \frac{1}{m}(\tilde{x}_3 + \tilde{x}_5 + \tilde{x}_7 + \tilde{x}_9) \\
\dot{\tilde{x}}_3 &= -l_2 \tilde{x}_2 + \gamma^2 \nu \tilde{x}_4 - e_2 \\
\dot{\tilde{x}}_4 &= -\nu \tilde{x}_3 \\
\dot{\tilde{x}}_5 &= -l_3 \tilde{x}_2 + 4\gamma^2 \nu \tilde{x}_6 - e_2 \\
\dot{\tilde{x}}_6 &= -\nu \tilde{x}_5 \\
\dot{\tilde{x}}_7 &= -l_4 \tilde{x}_2 + 9\gamma^2 \nu \tilde{x}_8 - e_2 \\
\dot{\tilde{x}}_8 &= -\nu \tilde{x}_7 \\
\dot{\tilde{x}}_9 &= -l_5 \tilde{x}_2 + 16\gamma^2 \nu \tilde{x}_{10} - e_2 \\
\dot{\tilde{x}}_{10} &= -\nu \tilde{x}_9
\end{aligned} \tag{24}$$

where $e_1 = x^* - x$, $e_2 = \dot{x}^* - \nu$, and $\tilde{x}_i = \hat{x}_i - x_i$.

Consider the following candidate Lyapunov function:

$$\begin{aligned}
V(\boldsymbol{e}, \tilde{\boldsymbol{x}}) = \frac{1}{2}\big(&\alpha e_1^2 + m e_2^2 + \beta m \tilde{x}_2^2 + \tilde{x}_3^2 + \gamma^2 \tilde{x}_4^2 + \tilde{x}_5^2 \\
&+ 4\gamma^2 \tilde{x}_6^2 + \tilde{x}_7^2 + 9\gamma^2 \tilde{x}_8^2 + \tilde{x}_9^2 + 16\gamma^2 \tilde{x}_{10}^2\big).
\end{aligned} \tag{25}$$

TABLE I
RATINGS AND KNOWN PARAMETERS OF LHSM UNDER TEST

Ratings and Parameters	Value
Pole Pitch	1.0 [mm]
Coil Resistance	1.4 [Ω]
Self Inductance	1.7 [mH]
Mover Mass	2.3 [kg]
Permanent Magnet	NdFeB (1.145[T])
Rated Static Force	40 [N]

The time derivative of V is given by

$$\dot{V}(\boldsymbol{e},\tilde{\boldsymbol{x}}) = -mk_1e_2^2 - \beta ml_1\tilde{x}_2^2 + (\alpha - mk_2)e_1e_2 + (\beta - l_2)\tilde{x}_2\tilde{x}_3 + (\beta - l_3)\tilde{x}_2\tilde{x}_5 + (\beta - l_4)\tilde{x}_2\tilde{x}_7 + (\beta - l_5)\tilde{x}_2\tilde{x}_9. \quad (26)$$

Then, there exist positive constants α and β such that

$$k_2 = \frac{\alpha}{m}$$
$$l_2 = l_3 = l_4 = l_5 = \beta \quad (27)$$

which leads to

$$\dot{V}(\boldsymbol{e},\tilde{\boldsymbol{x}}) = -mk_1e_2^2 - \beta ml_1\tilde{x}_2^2 < 0. \quad (28)$$

Thus, it can be concluded that the stability of the closed-loop system combining the controller and observer is guaranteed in the proposed scheme.

IV. EXPERIMENTAL RESULTS

A 1-mm-pole-pitch LHSM in Table I is tested to prove the validity of the proposed method. The PWM VSI inverter used here consists of 20-kHz switching devices and is controlled by a control board using a digital signal processor TMS320VC33. The sampling period of current and position is 50 and 500 μs, respectively. The Jacobian observer and linearization controller are performed every 50 and 500 μs, respectively. The linear encoder with 2000-pulse/pitch resolution is attached to the motor for the closed-loop position control. An ADXL-103 accelerometer from analog devices, with a maximum level of ± 1.7 g (1 g $= 9.8$ m/s^2) and 2.5-kHz frequency range, is mounted on the moving plate just to monitor the actual motor force.

Usually, estimator poles can be chosen to be reasonably faster than controller poles. This is to ensure the faster decay of estimator errors, as compared with the desired dynamics. From this specification, in the test, poles of the controller and observer are set to 200 and 5000 rad/s, respectively.

Fig. 6 shows the steady-state performance at 10 mm/s without the ripple force suppression control. In the test, the velocity level is chosen to be low enough to ensure that the vibration is not filtered out by the mechanical constant. From the top, velocity feedback, its FFT spectrum, the position error, and the motor force are depicted. From the FFT waveform, it is evident that the first-, second-, third-, and fourth-order harmonic components are dominant. The measurements show a good agreement with the reluctance network analysis. The frequency spectrum contains the higher order component than the fourth-order one. This component is mainly caused by unmodeled high-order terms in the permeance and the inverter dead-time effect.

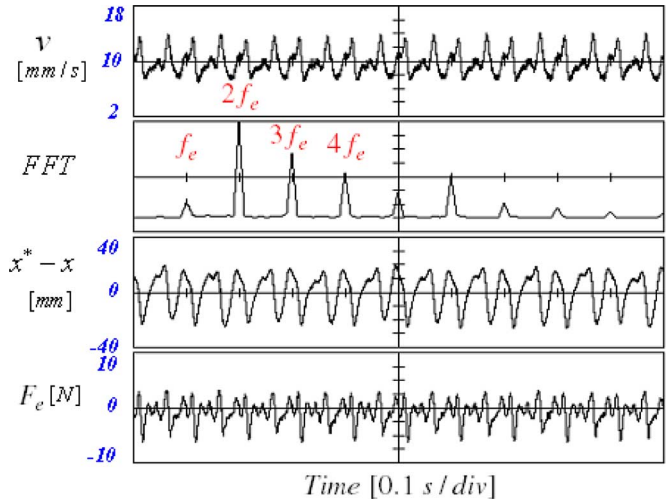

Fig. 6. Steady-state performance at 10 mm/s without the ripple force suppression.

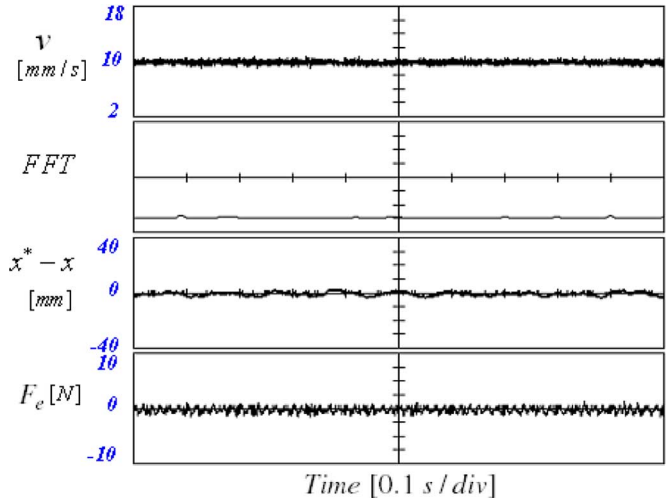

Fig. 7. Comparison of the results on the proposed ripple force rejection performance at 10 mm/s.

Fig. 7 shows a comparison result for the proposed ripple force rejection performance at 10 mm/s. The estimated disturbance is added to the overall input to cancel the effect of the ripple force in the feedforward manner. It makes a remarkable improvement for steady-state performance and the reduction of acoustic noise level. The experimental result shows that the proposed controller is able to effectively compensate the detent force, unbalanced effect, and other nonlinear characteristics of the LHSM. To assess how close the estimated force ripple matches the "true" one detected by the accelerometer, the two ripples are compared with each other, as illustrated in Fig. 8, where a close match is found except in the transient region. It is concluded that the proposed algorithm can provide a reliable estimation performance in a real situation.

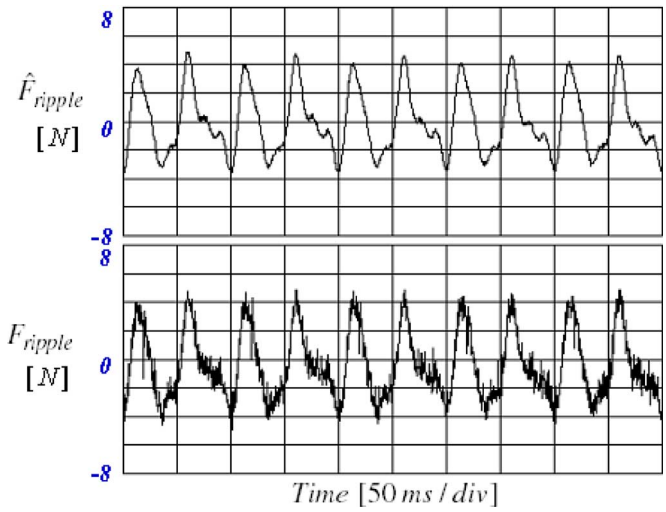

Fig. 8. Comparison between the measured and estimated ripple force.

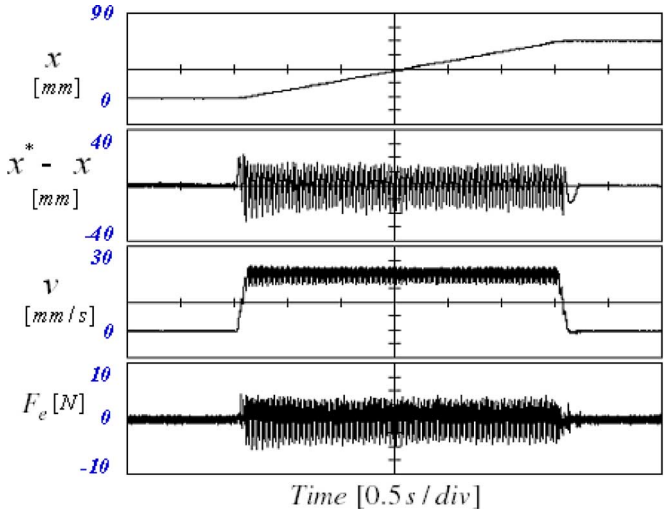

Fig. 9. Position tracking performance for PI controller alone.

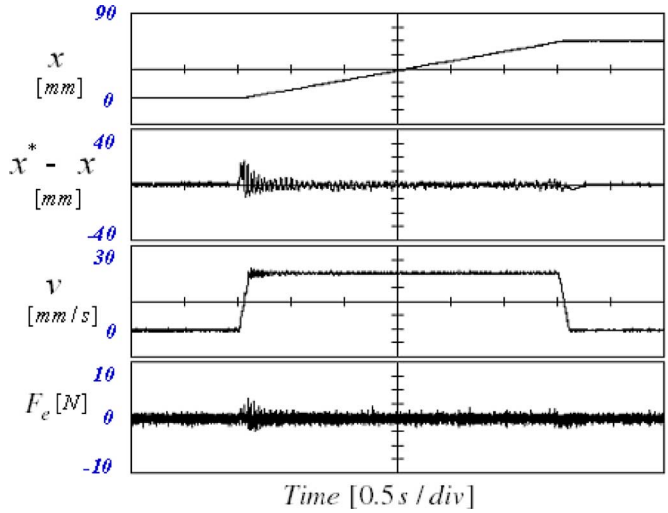

Fig. 10. Position tracking performance of proposed observer-based control scheme.

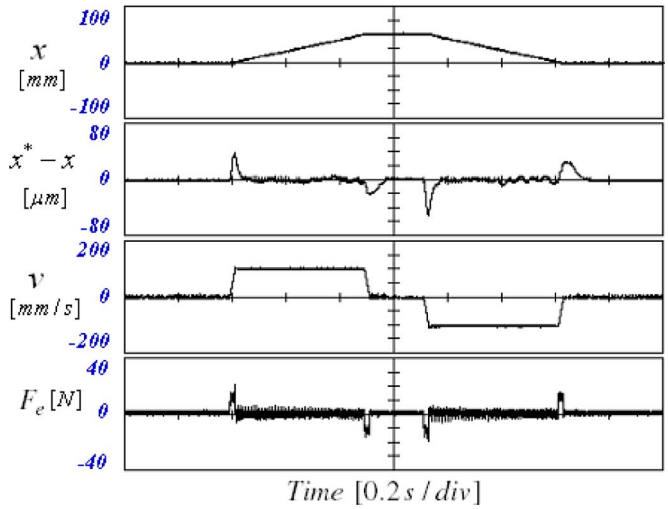

Fig. 11. Position tracking performance of proposed scheme at 100 mm/s.

Fig. 9 illustrates the position tracking performance of the linearization position/velocity controller without the ripple force compensation when the position command is changing from 0 to 60 mm. From the top, position feedback, position error, velocity, and motor force are depicted. The position errors of more than ± 20 μm can be seen, which are unacceptable in general servo applications. The force is still fluctuating, and this effect results in the acoustic noise emissions during operation.

Fig. 10 shows the position tracking performance of the proposed observer-based control scheme of mitigating the ripple force. Compared to the case with PI compensation, the tracking errors show that the maximum amplitude greatly reduced to less than ± 2.5 μm.

Fig. 11 illustrates a demonstration of the control performance of the proposed control scheme when the motor is running 100 mm/s. This result shows that the proposed algorithm yields a satisfactory high-speed control performance while restraining the thrust ripple. Positioning accuracy, which is within the limits of the servo applications, can be achieved using the proposed compensation method. This is considered a very significant performance improvement by high-performance servodrive makers.

V. Conclusion

This paper demonstrates an observer-based approach to compensate the inherent mechanical vibration of position-controlled LHSM drives. The LHSM with force ripple components is modeled as a nonlinear position-dependent function via an elaborate reluctance network analysis that incorporates the factors of magnetic coupling and nonlinear material properties. The Jacobian observer offers states estimates for the linearization feedback and position tracking. As the general separation principle is not available for nonlinear systems, the stability of the closed-loop system, including the observer and the controller, is verified through the Lyapunov method. From the experimental results, it is concluded that the proposed method can cope well with the ripple force problem of the LHSM drive. It is effective even when the LHSM is applied in servo control applications.

REFERENCES

[1] B. C. Kuo, *Theory and Applications of Step Motors*. St. Paul, MN: West, 1974.

[2] S. Yang, F. Lin, and M. Chen, "Micro-stepping control of a two-phase linear stepping motor with three-phase VSI inverter for high-speed applications," *IEEE Trans. Ind. Appl.*, vol. 40, no. 5, pp. 1257–1264, Sep./Oct. 2004.

[3] J. K. Seok and T. S. Hwang, "Cogging force reduction of two phase linear hybrid stepping motor," *IEEE Trans. Magn.*, vol. 41, no. 6, pp. 2202–2204, Jun. 2005.

[4] J. Hirai, T. Kim, and A. Kawamura, "Position-sensorless drive of linear pulse motor for suppressing transient vibration," *IEEE Trans. Ind. Electron.*, vol. 47, no. 2, pp. 337–345, Apr. 2000.

[5] J. B. Grimbleby, "Simple algorithm for closed-loop control of stepping motors," *Proc. Inst. Electr. Eng.—Electr. Power Appl.*, vol. 142, no. 1, pp. 5–13, Jan. 1995.

[6] T. S. Hwang, J. K. Seok, and D. H. Kim, "High performance control of $\pi/4$-multiple-pitched linear hybrid stepping motor with ripple force compensator," *IEEE Trans. Magn.*, vol. 42, no. 2, pp. 329–334, Feb. 2006.

[7] J. K. Seok, T. S. Hwang, and D. H. Kim, "Initial position estimation for closed-loop linear hybrid stepping motor drives using DC excitation," *IEEE Trans. Magn.*, vol. 42, no. 8, pp. 2071–2076, Aug. 2006.

[8] N. H. Jo and J. H. Seo, "A state observer for nonlinear systems and its application to ball and beam system," *IEEE Trans. Autom. Control*, vol. 45, no. 5, pp. 968–973, May 2000.

[9] H. K. Khalil, *Nonlinear Systems*. Englewood Cliffs, NJ: Prentice-Hall, 1996.

[10] B. de Jager, "Improving the tracking performance of mechanical systems by adaptive extended friction compensation," *Control Eng. Pract.*, vol. 1, no. 6, pp. 1009–1018, 1993.

[11] M. A. Rahman and M. A. Hoque, "On-line self-tuning ANN-based speed control of a PM DC motor," *IEEE/ASME Trans. Mechatronics*, vol. 2, no. 3, pp. 169–178, Sep. 1997.

[12] A. N. Atassi and H. K. Khalil, "A separation principle for the stabilization of a class of nonlinear systems," *IEEE Trans. Autom. Control*, vol. 44, no. 9, pp. 1672–1687, Sep. 1999.

Tai-Sik Hwang (S'04) received the B.S. and M.S. degrees in electrical engineering from Yeungnam University, Kyungbuk, Korea, in 2004 and 2006, respectively.

He is currently with Robostar Company Ltd., Anyang, Korea. His specific research interest is in high-performance electrical machine drives.

Jul-Ki Seok (S'94–M'98) received the B.S., M.S., and Ph.D. degrees in electrical engineering from Seoul National University, Seoul, Korea, in 1992, 1994, and 1998, respectively.

From 1998 to 2001, he was a Senior Engineer in the Production Engineering Center, Samsung Electronics, Suwon, Korea. Since 2001, he has been a member of the faculty of the School of Electrical Engineering, Yeungnam University, Gyeongsan, Korea, where he is currently an Associate Professor. His specific research interests are in high-performance electrical machine drives, sensorless control of ac machines, and nonlinear system identification related to the power electronics field.